Developmental Cell
Article

Endocytic Pathways Downregulate the L1-type Cell Adhesion Molecule Neuroglian to Promote Dendrite Pruning in *Drosophila*

Heng Zhang,[1,6] Yan Wang,[1,2,6] Jack Jing Lin Wong,[1,2] Kah-Leong Lim,[3,4,5] Yih-Cherng Liou,[1] Hongyan Wang,[2,3,5] and Fengwei Yu[1,2,3,*]

[1]Temasek Life Sciences Laboratory and Department of Biological Sciences, National University of Singapore, 1 Research Link, Singapore 117604, Singapore
[2]NUS Graduate School for Integrative Sciences and Engineering, Centre for Life Sciences, Singapore 117456, Singapore
[3]Neuroscience and Behavioural Disorders Program, Duke-NUS Graduate Medical School, Singapore 169857, Singapore
[4]National Neuroscience Institute, Singapore 308433, Singapore
[5]Department of Physiology, National University of Singapore, Singapore 117597, Singapore
[6]Co-first author
*Correspondence: fengwei@tll.org.sg
http://dx.doi.org/10.1016/j.devcel.2014.06.014

SUMMARY

Pruning of unnecessary axons and/or dendrites is crucial for maturation of the nervous system. However, little is known about cell adhesion molecules (CAMs) that control neuronal pruning. In *Drosophila*, dendritic arborization neurons, ddaCs, selectively prune their larval dendrites. Here, we report that Rab5/ESCRT-mediated endocytic pathways are critical for dendrite pruning. Loss of *Rab5* or *ESCRT* function leads to robust accumulation of the L1-type CAM Neuroglian (Nrg) on enlarged endosomes in ddaC neurons. Nrg is localized on endosomes in wild-type ddaC neurons and downregulated prior to dendrite pruning. Overexpression of Nrg alone is sufficient to inhibit dendrite pruning, whereas removal of Nrg causes precocious dendrite pruning. Epistasis experiments indicate that Rab5 and ESCRT restrain the inhibitory role of Nrg during dendrite pruning. Thus, this study demonstrates the cell-surface molecule that controls dendrite pruning and defines an important mechanism whereby sensory neurons, via endolysosomal pathway, downregulate the cell-surface molecule to trigger dendrite pruning.

INTRODUCTION

A critical step in the establishment of the mature nervous system is selective removal of exuberant or unnecessary neuronal processes without death of the parental neurons, referred to as pruning (Luo and O'Leary, 2005). In mammals, neurons located in the cortical layer V (O'Leary and Koester, 1993) and hippocampal dentate gyrus (Bagri et al., 2003; Riccomagno et al., 2012) prune inappropriate and exuberant axon branches to form proper connectivity. In *Drosophila*, many neurons selectively prune their larval dendrites and/or axons during metamorphosis (Schubiger et al., 1998; Truman, 1990). In the CNS, mushroom body (MB) γ neurons eliminate their dorsal and medial axon branches via local degeneration and glia-mediated engulfment (Awasaki and Ito, 2004; Lee et al., 2000; Watts et al., 2003). In the peripheral nervous system, dorsal dendritic arborization (dda) neurons, ddaD/E (class I) and ddaC (class IV), specifically prune their larval dendritic arbors with axons intact and regenerate adult-specific dendrites (Kuo et al., 2005; Williams and Truman, 2005), whereas ddaF neurons (class III) undergo apoptosis during the first day of metamorphosis (Williams and Truman, 2005). In *C. elegans*, excessive neuronal processes connecting two AIM interneurons are eliminated during the larval stages (Kage et al., 2005). Thus, neuronal pruning is a common strategy to remodel the developing nervous systems across species.

Drosophila ddaC sensory neurons have emerged as an attractive model to study cellular and molecular mechanisms of dendrite-specific pruning. In response to a late larval pulse of the steroid-molting hormone 20-hydroxyecdysone (ecdysone), dendrite pruning is initiated in ddaC neurons, involving severing of proximal dendrites, rapid fragmentation of detached dendrites, and clearance of dendritic debris (Figure 1A; Kuo et al., 2005; Williams and Truman, 2005). The ecdysone receptor (EcR-B1) and its coreceptor Ultraspiracle act together with two epigenetic factors Brahma and CREB-binding protein to activate the common downstream gene *sox14* and induce the onset of dendrite pruning (Kirilly et al., 2009, 2011). Other molecules and pathways, such as ubiquitin-proteasome system (Kuo et al., 2006; Wong et al., 2013), caspases (Kuo et al., 2006; Williams et al., 2006), Ik2/Kat60L (Lee et al., 2009), Mical (Kirilly et al., 2009), headcase (Loncle and Williams, 2012), calcium signaling (Kanamori et al., 2013), and the insulin pathway (Wong et al., 2013), also regulate dendrite pruning in ddaC neurons.

Endocytic pathways regulate turnover and homeostasis of cell-surface receptors and attenuation of signaling pathways in unicellular and multicellular organisms (Raiborg and Stenmark, 2009; Zerial and McBride, 2001). Ubiquitinated membrane proteins are endocytosed from the plasma membrane to endocytic vesicles, which are fused with early endosomes. The key small guanosine triphosphatase Rab5 regulates formation, fusion, and sorting of early endosomes. Early endosomes are further transported via several downstream trafficking routes, one of

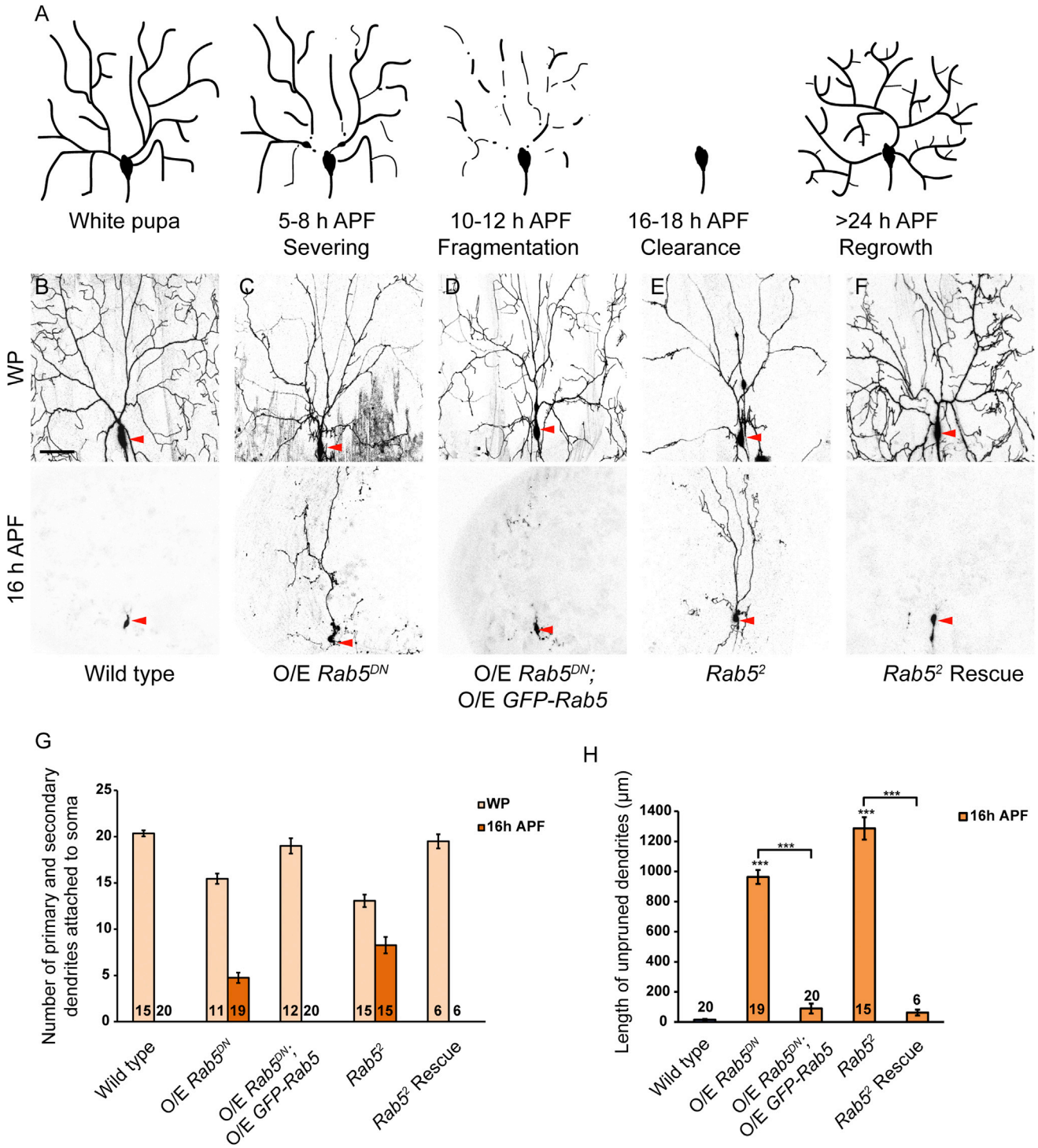

Figure 1. Rab5-Dependent Early Endocytic Pathway Is Critical for Dendrite Pruning in ddaC Neurons

(A) A schematic representation of dendrite pruning in ddaC neurons.

(B–F) Dendrites of wild-type (B), Rab5^{DN}-expressing (C), Rab5^{DN} and GFP-Rab5-coexpressing (D), *Rab5^{2}* MARCM (E), and *Rab5^{2}* rescue (F) ddaC neurons at WP and 16 hr APF stages. Red arrowheads point to the ddaC somas.

(G) Quantification of the average number of primary and secondary ddaC dendrites.

(H) Quantification of the total length of unpruned ddaC dendrites.

Error bars represent SEM. The scale bar represents 50 μm. See genotypes of fly strains in Supplemental Experimental Procedures. See also Figure S1.

which is maturation into multivesicular bodies (MVBs) (or multivesicular endosomes) in a process dependent on the endosomal sorting complexes required for transport (ESCRT) (Figure S1A available online). MVBs subsequently form late endosomes and fuse with lysosomes to degrade their contents (Figure S1A; Rusten et al., 2012). In postmitotic neurons, endocytic pathways play important roles in a number of cellular and physiological processes, such as axon guidance, dendrite morphogenesis, synaptic vesicle trafficking, synaptic plasticity, and neuronal migration (Dittman and Ryan, 2009; Kennedy and Ehlers, 2006; Yap and Winckler, 2012). Endocytosis and endosomal trafficking regulate dendritic growth and branching pattern in *Drosophila* sensory neurons during larval stages (Satoh et al., 2008; Sweeney et al., 2006; Yang et al., 2011). Loss of Rab5 leads to simplified dendrite arbors in ddaC neurons (Satoh et al., 2008), whereas loss of the ESCRT components causes increased branching complexity along the proximal-distal axis in the class IV da neurons (Sweeney et al., 2006). It has been proposed that, at the larval stages, Rab5-containing endosomal cargoes promote branch formation, whereas the ESCRT complex can facilitate lysosomal degradation of the endosomal cargoes, thereby inhibiting branch formation (Satoh et al., 2008). In contrast, endocytosis also regulates collapse of axonal growth cone during axon guidance by removal of cell-surface membrane receptors (Fournier et al., 2000), for example, semaphorin3A-induced endocytosis of neuropilin1 (Castellani et al., 2004). However, to our knowledge, a cell-autonomous role of endocytic pathways in remodeling neurons has not yet been documented in *Drosophila*. Moreover, a functional link between endocytic pathways and cell-surface molecules in regulating neuronal pruning remains unknown.

Here, we report that Rab5-dependent early endocytic and ESCRT-dependent MVB maturation pathways play crucial roles in dendrite pruning of ddaC sensory neurons. We have further identified the *Drosophila* L1-type cell adhesion molecule (CAM) Nrg, which is downregulated by Rab5 and ESCRT in ddaC neurons prior to dendrite pruning. Nrg plays an inhibitory role in dendrite pruning of ddaC neurons. Thus, this study demonstrates an important role of endocytic pathways in downregulating Nrg to facilitate dendrite pruning in sensory neurons.

RESULTS

Rab5-Dependent Early Endocytic Pathway Is Critical for Dendrite Pruning

In a large-scale RNAi screen searching for regulators of ddaC dendrite pruning (Y.W., H.Z., and F.Y., unpublished data), we isolated two independent RNAi transgenes, v103945 and v34096 (Dietzl et al., 2007), corresponding to the same gene *Rab5*. RNAi knockdown of *Rab5,* via the class IV da neuron driver *ppk-Gal4* (Grueber et al., 2003), led to consistent dendrite-pruning defects in the majority of ddaC neurons at 16 hr after puparium formation (APF) (n = 16 and 15, respectively; Figure S1B; data not shown). In contrast, all larval dendrites were completely pruned in the control neurons at this stage (n = 20; Figure S1B). Rab5 converts between an inactive guanosine diphosphate (GDP)-bound form and an active guanosine-triphosphate-bound form (Zerial and McBride, 2001). We therefore expressed $Rab5^{S43N}$, a dominant-negative and GDP-bound form of Rab5 (hereafter referred to as $Rab5^{DN}$; Entchev et al., 2000), in ddaC neurons. The expression of $Rab5^{DN}$, via four copies of *ppk-Gal4* driver, resulted in prominent dendrite-severing defects with the persistence of 5.2 primary and secondary dendrites at 16 hr APF and 963 μm of unpruned dendrites in ddaC neurons (n = 19; 100%; Figures 1C, 1G, and 1H), which were rescued by coexpression of GFP-Rab5 (n = 20; Figures 1D, 1G, and 1H).

To further confirm the requirement of *Rab5* function for dendrite pruning, we generated homozygous mosaic analysis with a repressible cell marker (MARCM) clones (Lee and Luo, 1999) using the null allele $Rab5^{2}$ (Wucherpfennig et al., 2003). On average, 8.3 of primary and secondary dendrites and 1,286 μm of unpruned dendrites persisted in $Rab5^{2}$ mutant ddaC clones by 16 hr APF (n = 15; 100%; Figures 1E, 1G, and 1H). The larval dendrites in all $Rab5^{2}$ clones were present by 24 hr APF (n = 8; data not shown) and eventually removed by 32 hr APF (n = 7; data not shown), presumably due to extensive migration and apoptosis in the abdominal epidermis on which the dendrites elaborate (Williams and Truman, 2005). The dendrite-pruning defects in $Rab5^{2}$ ddaC neurons were rescued at 16 hr APF by reintroduction of Rab5 (n = 6; Figures 1F, 1G, and 1H). We then examined the potential involvement of Avalanche (Avl), an early endosomal syntaxin (Lu and Bilder, 2005), which also regulates early endosomal fusion (Jahn et al., 2003). Interestingly, ddaC MARCM clones of the null allele avl^{1} exhibited consistent dendrite-pruning defects in all mutant neurons by 16 hr APF (n = 5; Figure S1C). Thus, the early endocytic regulators Rab5 and Avl are required to promote dendrite pruning in ddaC neurons. Consistent with the previous studies (Satoh et al., 2008), elaboration of high-order dendritic branches was severely affected in $Rab5^{DN}$ or $Rab5^{2}$ mutant ddaC neurons (Figures 1C and 1E). The numbers of primary and secondary dendrites at the white prepupal (WP) stage were also reduced in these mutant ddaC neurons (Figure 1G). To rule out the possibility that the $Rab5^{DN}$ dendrite-pruning defect is a secondary effect of the initial morphology defect, we induced $Rab5^{DN}$ expression at the early third instar larval stage using the Gene-Switch system, which did not affect initial ddaC dendritic morphology (Figure S1D). Dendrite-pruning defects were observed in the $Rab5^{DN}$-expressing ddaC neurons derived from RU486-fed animals (50%; n = 32; Figure S1D), in contrast to no pruning defect observed in nonfed animals (n = 22; Figure S1D). In addition to ddaC neurons, wild-type ddaD/ddaE neurons also pruned their larval dendrites by 19 hr APF (n = 20; Figure S1E). In contrast, all ddaD/ddaE neurons derived from $Rab5^{2}$ MARCM clones retained most of their larval dendrites by 19 hr APF (n = 3; Figure S1E). Wild-type ddaF neurons are eliminated by apoptosis during early metamorphosis (Williams and Truman, 2005). Interestingly, ddaF neurons derived from either $Rab5^{2}$ or avl^{1} mutants were eliminated by 16 hr APF (n = 3 and 4, respectively; data not shown), similar to wild-type neurons (n = 5).

Collectively, Rab5-dependent early endocytic pathway is required for the regulation of dendrite pruning, but dispensable for apoptosis, in sensory neurons during early metamorphosis.

ESCRT-Dependent Endosomal Maturation Is Important for Dendrite Pruning

We next investigated potential involvement of MVB maturation, a trafficking route downstream of early endosomes, in ddaC

dendrite pruning. MVB maturation is dependent on the ESCRT complexes (Rusten et al., 2012). We examined several core components of the ESCRT complexes, such as Vps28 (ESCRT-I complex), Vps32 (also known as Shrub/Snf-7; ESCRT-III complex), and Vps4 (AAA ATPase required for disassembly of the ESCRT-III complex). MARCM analyses of the null allele $Vps32^{G5}$ (Vaccari et al., 2009) exhibited dendrite-severing defects in 87% of ddaC mutant clones (n = 23) and fragmentation defects in the rest of clones (data not shown). On average, 4.4 of larval dendrites and 796 μm of unpruned dendrites were still present at 16 hr APF (Figures 2B, 2E, and 2F) and eventually removed by 32 hr APF (n = 10; data not shown). ddaC MARCM clones of $Vps28^{B9}$, a null or strong allele (Vaccari et al., 2009), showed consistent dendrite-severing defects (62%; n = 13; Figure S2A) and fragmentation defects in the rest of clones (data not shown). The expression of Myc-tagged Vps32 or Vps28 rescued the dendrite-pruning defects in $Vp32^{G5}$ (n = 6; Figures 2C, 2E, and 2F) or $Vps28^{B9}$ (n = 3; Figure S2A) MARCM ddaC neurons at 16 hr APF, respectively. Moreover, overexpression of the dominant-negative construct Vps32-GFP (also known as Shrub-GFP; Sweeney et al., 2006) also caused similar severing defects in ddaC neurons (75%; n = 24; Figure S2A), resembling the *Vps32* loss-of-function phenotype. The expression of the Vps4 dominant-negative construct ($Vps4^{DN}$), which abolishes the AAA ATPase activity (Rusten et al., 2007), also led to retention of larval dendrites attached to ddaC neurons (n = 25; 72%; Figures 2D, 2E, and 2F). ddaC neurons derived from various *ESCRT* mutants exhibited dendritic overbranching phenotypes near their somas at WP stage (Figures 2B, 2D, and S2A), similar to that reported in *vps32/shrub* mutants (Sweeney et al., 2006). Moreover, via the Gene-Switch system, we induced $Vps4^{DN}$ expression at the late larval stage, which did not affect initial dendrite morphology at WP stage (n = 16). Importantly, the dendrite pruning defects were observed in the $Vps4^{DN}$-expressing ddaC neurons derived from RU486-fed animals (75%; n = 24; Figure S2B), in contrast to no pruning defect in nonfed controls (n = 15). Mutant ddaD/ddaE neurons, derived from $Vps28^{B9}$ (100%; n = 3), $Vps32^{G5}$ (100%; n = 4), or $Vps4^{DN}$ (100%; n = 28), retained some of their larval dendrites attached by 19 hr APF (Figure S2C). These ESCRT components, like Rab5, are dispensable for ddaF apoptosis (data not shown). Consistent with these observations, Rab5 and the ESCRT complexes are dispensable for EcR-B1 upregulation during the larval-pupal transition (data not shown). Thus, the ESCRT complexes, like Rab5, are required to regulate dendrite pruning, rather than apoptosis, in sensory neurons.

Taken together, Rab5/ESCRT-dependent endocytic pathways play cell-autonomous roles in the regulation of dendrite pruning in ddaC neurons.

Loss of *Rab5* or *ESCRT* Function Leads to Formation of Enlarged Endosomal Compartments and Aberrant Ubiquitinated Protein Deposits in ddaC Neurons

We next attempted to understand cellular mechanisms by which the endocytic pathways regulate ddaC dendrite pruning. We utilized the early endosomal marker Avl and the early/MVB endosomal markers Hrs/Vps28 to examine the distribution and size of endosomes in wild-type and mutant ddaC neurons. Wild-type ddaC neurons showed weak and discrete puncta of endosomal compartments positive for Avl (n = 8; Figure 3A) and Hrs (n = 8; Figure 3D). In contrast, both $Rab5^{2}$ and $Rab5^{DN}$ mutant ddaC neurons exhibited drastic aggregation of Avl (n = 4 and 12, respectively; Figures 3B and S3A), Hrs (n = 5 and 14, respectively; Figures 3E and S3A), and Vps28 (data not shown) signals in two or three intracellular structures with full penetrance, suggesting an enlargement of endosomes. Interestingly, these abnormal endosomes were also colabeled by the anti-ubiquitin antibody (n = 9 and 26, respectively, Figures 3B and S3A; wild-type, n = 8, Figure 3A). Moreover, Avl and ubiquitin staining revealed more robust accumulation of endosomal compartments and protein aggregates in $Vps32^{G5}$ MARCM (100%; n = 4; Figure 3C), $Vps4^{DN}$-expressing (100%; n = 10; Figure S3A), or $Vps28^{B9}$ MARCM (100%; n = 4; Figure S3A) ddaC neurons. Similarly, Hrs (n = 3, 10, and 3, respectively; Figures 3F and S3A) and Vps28 (data not shown) also labeled a number of enlarged endosomes in various *ESCRT* mutant ddaC neurons. These data indicate that loss of *Rab5* or *ESCRT* function disrupts normal distribution of endosomal compartments and removal of ubiquitinated proteins in ddaC neurons. We coexpressed $Rab5^{DN}$ with $Vps4^{DN}$ in ddaC neurons, which resulted in two or three enlarged endosomes positive for Avl, ubiquitin, and Hrs (Figure S3A), indistinguishable from $Rab5^{DN}$ alone, suggesting that *Rab5* is epistatic to *Vps4*. Thus, Rab5 and the ESCRT complexes regulate endosomal trafficking and removal of ubiquitinated proteins in ddaC neurons. Moreover, when $Rab5^{DN}$ or $Vps4^{DN}$ expression was induced at the late larval stage via the Gene-Switch system, we also observed colocalization of enlarged endosomes with robust ubiquitin (Ubi) aggregates at 6 hr APF (Figure S5A). The percentages of these enlarged endosomes are 62% in $Rab5^{DN}$ (n = 13) and 79% in $Vps4^{DN}$ (n = 19) mutant neurons, correlating with their pruning phenotypes (50% and 75%, respectively) in Figures S1D and S2B. We observed smaller or weaker endosomes with lower Ubi aggregates at WP stage in these $Rab5^{DN}$ or $Vps4^{DN}$ mutant neurons (Figure S5A).

We then confirmed whether these enlarged endosomes are incompetent for lysosomal fusion. We first used lysosome-associated membrane protein 1 fused to GFP (LAMP1-GFP), a marker labeling both late endosomes and lysosomes. LAMP1-GFP was separately distributed in wild-type ddaC neurons (n = 12; Figure 3G). In contrast, LAMP1-GFP accumulated on the enlarged ubiquitin-positive endosomes in $Rab5^{DN}$ (100%; n = 20; Figure 3H) or $Vps4^{DN}$ (100%; n = 10; Figure 3I) ddaC neurons, suggesting that the identity of these structures is either MVB/late endosome or lysosome. To specifically label lysosomes, we made use of the fluorescent LysoTracker, a membrane-permeable dye labeling highly acidified lysosomal compartments. In wild-type ddaC neurons, the LysoTracker staining marked lysosomes also positive for LAMP1-GFP (n = 13; Figure 3J). In contrast, the LysoTracker dye failed to stain the enlarged LAMP1-positive endosomes in $Rab5^{DN}$ (n = 8; Figure 3K) or $Vps4^{DN}$ (n = 10; Figure 3L) ddaC neurons, suggesting a failure of fusion between late endosomes and lysosomes. Thus, the formation of the enlarged endosomes in *Rab5* or *ESCRT* mutant ddaC neurons are possibly due to impaired membrane invagination and abnormal endosomal maturation (Lloyd et al., 2002). Thus, the endolysosomal pathway is disrupted in mutant ddaC neurons devoid of *Rab5* or *ESCRT* function, resulting in drastic protein accumulation. In addition, loss of

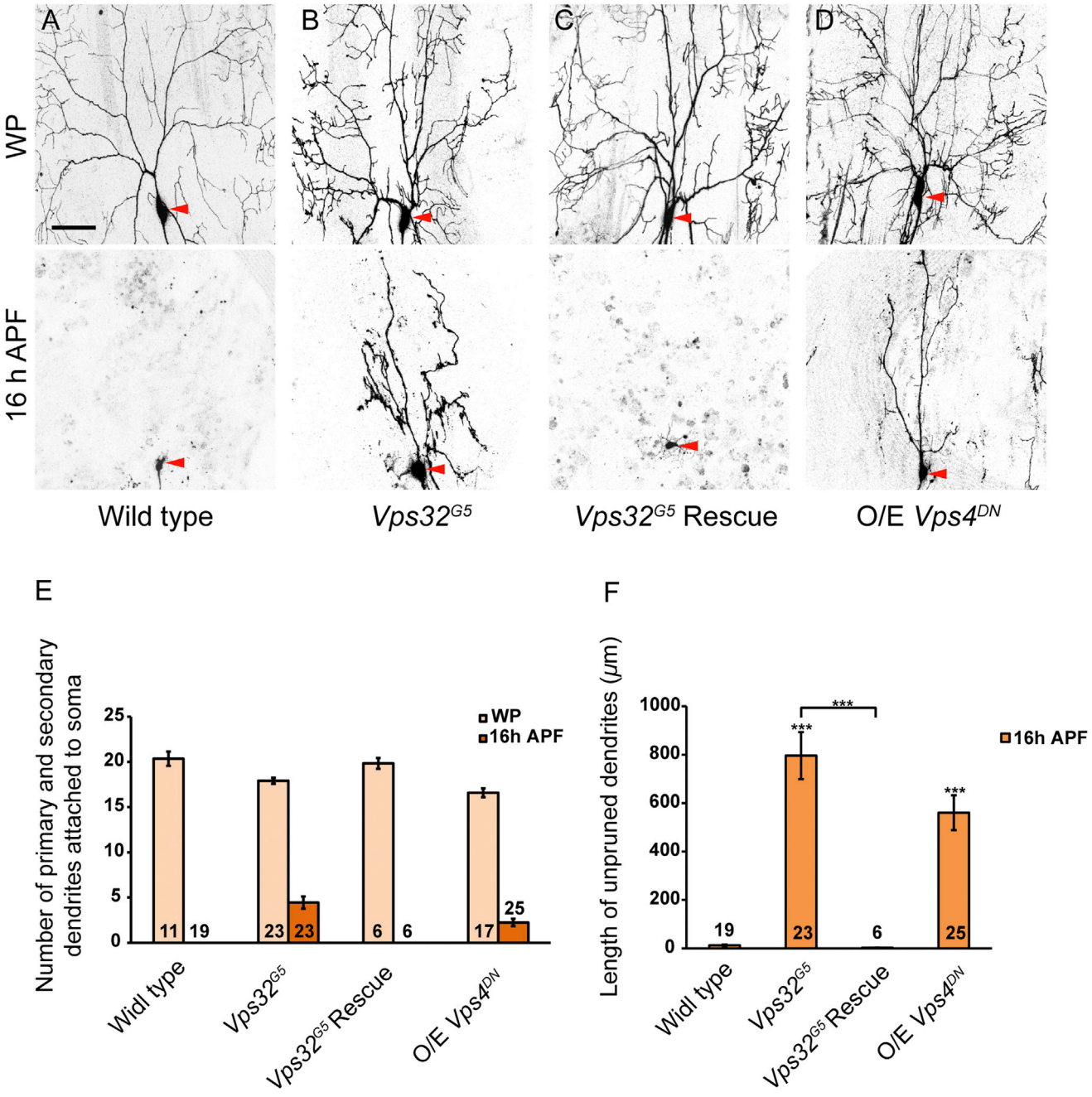

Figure 2. ESCRT-Dependent Endosomal Maturation Is Important for Dendrite Pruning in ddaC Neurons

(A–D) Dendrites of wild-type (A), *Vps32*^{G5} MARCM (B), *Vps32*^{G5} rescue (C), and Vps4^{DN}-expressing (D) ddaC neurons at WP and 16 hr APF stages. Red arrowheads point to the ddaC somas.

(E) Quantification of the average number of primary and secondary ddaC dendrites.

(F) Quantification of the total length of unpruned ddaC dendrites.

Error bars represent SEM. The scale bar represents 50 μm. See genotypes of fly strains in Supplemental Experimental Procedures. See also Figure S2.

Rab5 or *ESCRT* function did not disturb distribution of the mitochondrial marker Mito-GFP (Figure S3B), the *cis*-Golgi matrix protein GM130 (Figure S3C), and the ER marker KDEL (Figure S3D).

Taken together, Rab5/ESCRT-dependent endocytic pathways actively regulate protein turnover in ddaC neurons.

Cell-Surface Molecules Nrg, Robo, and N-Cad Robustly Accumulate on the Enlarged Endosomes in *Rab5* or *ESCRT* Mutant ddaC Neurons

Endocytosis of cell-surface receptors has been reported to be an important mechanism for attenuation of various signaling pathways during development (Ceresa and Schmid, 2000). In

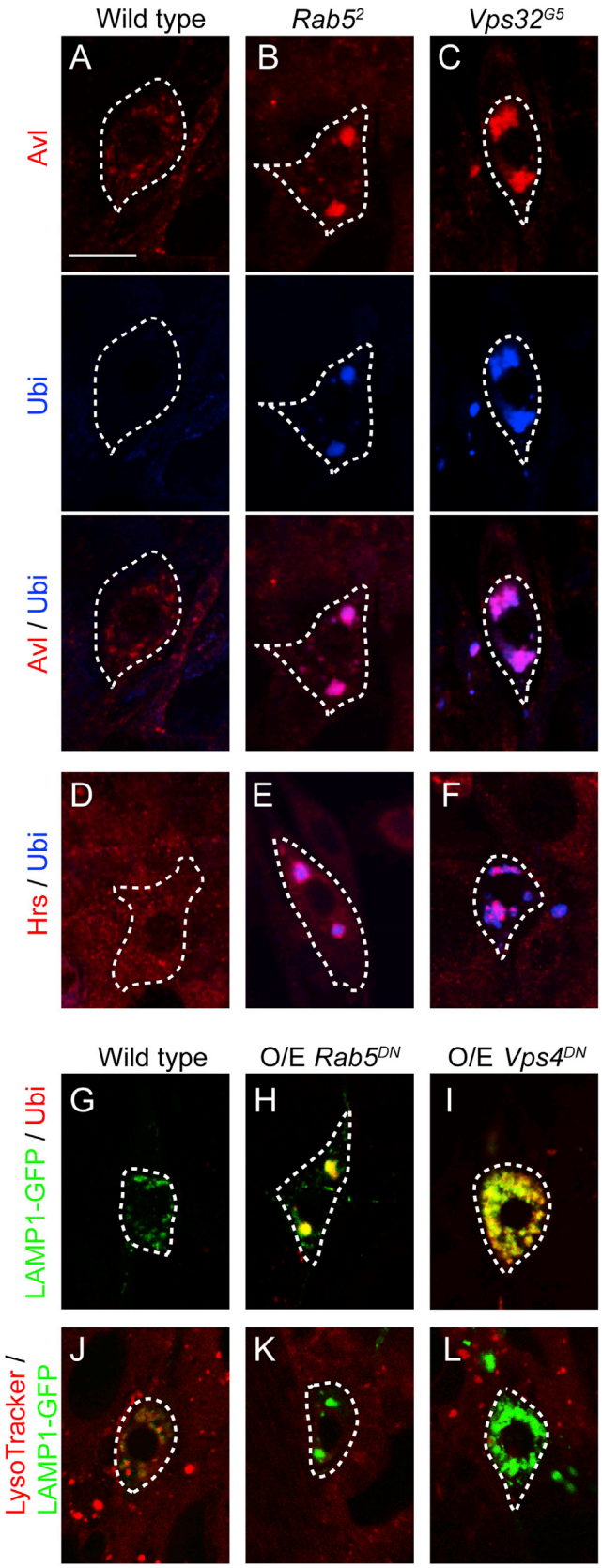

Figure 3. Loss of *Rab5* or *ESCRT* Function Leads to Formation of Enlarged Endosomal Compartments and Aberrant Ubiquitinated Protein Deposits in ddaC Neurons

(A–C) The distribution of Avl and ubiquitinated protein deposits in wild-type (A), $Rab5^{2}$ (B), or $Vp32^{G5}$ (C) MARCM ddaC neurons.

(D–F) The distribution of Hrs protein in wild-type (D), $Rab5^{2}$ (E), or $Vp32^{G5}$ (F) MARCM ddaC neurons.

(G–I) The distribution of LAMP1-GFP in wild-type (G), $Rab5^{DN}$ (H), or $Vps4^{DN}$ (I) ddaC neurons.

(J–L) The distribution of LysoTracker in wild-type (J), $Rab5^{DN}$ (K), or $Vps4^{DN}$ (L) ddaC neurons. ddaC somas are marked by dashed lines.

Error bars represent SEM. The scale bar represents 10 μm. See genotypes of fly strains in Supplemental Experimental Procedures. See also Figure S3.

Drosophila imaginal discs, loss of *Rab5* or *ESCRT* function causes accumulation of receptors/ligands on enlarged endosomes and upregulation of their downstream signaling pathways, including Notch, Wingless, Dpp, epidermal growth factor receptor, TKR, PVR, or Hedgehog (Herz et al., 2006; Lloyd et al., 2002; Lu and Bilder, 2005; Thompson et al., 2005; Vaccari and Bilder, 2005). Surprisingly, both Rab5 and ESCRT are not required to modulate these signaling pathways during ddaC dendrite pruning. First, their known receptors/ligands did not accumulate on enlarged endosomes in $Rab5^{DN}$, $Vps4^{DN}$, or $Vps32^{G5}$ ddaC neurons (Table S1; data not shown). Second, several major downstream effectors or LacZ reporters examined were not affected in $Rab5^{DN}$ or $Vps4^{DN}$ ddaC neurons (Table S1; data not shown). Finally, attenuation of these signaling pathways did not suppress or enhance $Rab5^{DN}$-associated ddaC dendrite pruning defects (Table S2; data not shown).

To identify cell-surface molecules that are accumulated on the enlarged endosomes in *Rab5* or *ESCRT* mutant ddaC neurons, we conducted an antibody-based screen using a number of monoclonal antibodies against transmembrane proteins, commercially available from DSHB. Among 45 transmembrane proteins examined, Nrg, Roundabout (Robo), and N-cadherin (N-Cad) exhibited prominent accumulations on the enlarged endosomes in *Rab5* or *ESCRT* mutant ddaC neurons. The neuron-specific isoform of Nrg (known as Nrg180), which is specifically detected by the BP104 antibody, was localized at somas, dendrites, and axons of ddaC (n = 10; Figure 4A) and other da neurons at the wandering third instar larval (wL3) stage in wild-type (Yamamoto et al., 2006; Yang et al., 2011). Importantly, Nrg exhibited robust aggregation on the enlarged endosomes in $Rab5^{DN}$ or $Rab5^{2}$ MARCM mutant ddaC neurons with full penetrance (n = 14 and 12, respectively; Figures 4B and 4C), colocalizing with the early endosomal marker Avl (Figures 4B and 4C) and ubiquitin (data not shown). In addition to the endosomal accumulation, we also observed 1.5-fold increases in Nrg protein levels around the soma cortex at wL3 stage (Figures 4B and 4C), presumably due to clog up of Nrg on the plasma membrane. The endosomal Nrg aggregates are specific, as Nrg RNAi knockdown completely eliminated the Nrg signals from Avl-positive endosomes in $Rab5^{DN}$ ddaC neurons (n = 5; Figure 4D). Thus, these data indicate a severe defect in endosomal trafficking of Nrg in *Rab5* mutant ddaC neurons. In contrast, Robo and N-Cad were accumulated on the enlarged endosomal compartments, but not on the cell surface, in all $Rab5^{2}$ MARCM (n = 3 and 3; Figures S4A and S4B) or $Rab5^{DN}$ (Figures S4C and S4D) mutant ddaC neurons, whereas both proteins were weakly

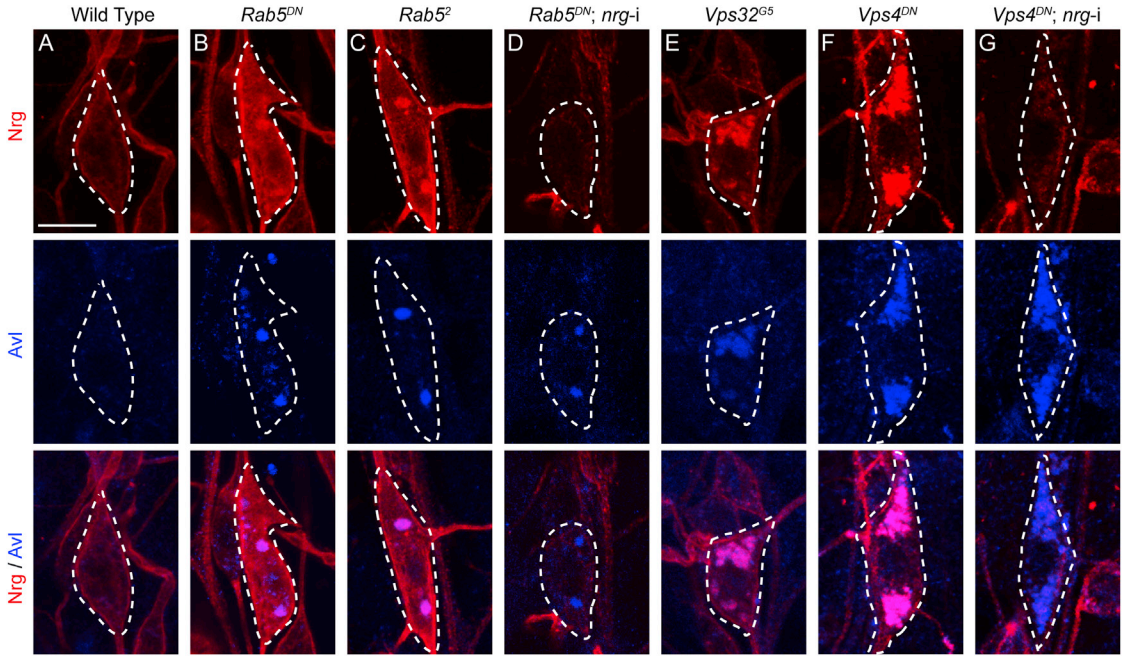

Figure 4. The Cell-Surface Molecule Nrg Robustly Accumulates on the Enlarged Endosomes in *Rab5* or *ESCRT* Mutant ddaC Neurons
The distribution of Nrg and Avl in wild-type (A), $Rab5^{DN}$ (B), $Rab5^{2}$ (C), $Rab5^{DN}$ expression with *nrg* RNAi knockdown (D), $Vp32^{G5}$ (E), $Vps4^{DN}$ (F), or $Vps4^{DN}$ expression with *nrg* RNAi knockdown (G) ddaC neurons. ddaC somas are marked by dashed lines. Error bars represent SEM. The scale bar represents 10 μm. See genotypes of fly strains in Supplemental Experimental Procedures. See also Figure S4 and Tables S1 and S2.

expressed without detectable membrane-associated signals in the wild-type neurons (n = 10 and 10; Figures S4A and S4B). These Robo or N-Cad aggregates were eliminated by their respective RNAi knockdowns in $Rab5^{DN}$ ddaC neurons (n = 6 and 6, respectively; Figures S4C and S4D). Likewise, Nrg, Robo, and N-Cad exhibited more robust accumulations on the endosomal compartments in all $Vps32^{G5}$ MARCM (n = 8, 3, and 5, respectively; Figures 4E, S4A, and S4B), $Vps4^{DN}$-expressing (n = 10; Figure 4F; data not shown), or $Vps28^{B9}$ MARCM (n = 6, 3, and 5, respectively; Figures S4A and S4B; data not shown) ddaC neurons at wL3 stage. Nrg RNAi knockdown efficiently eliminated endosomal Nrg signals in $Vps4^{DN}$ ddaC neurons (n = 10; Figure 4G). In contrast, other membrane proteins, mCD8GFP and the CAMs integrins, were not enriched on the enlarged endosomes in $Rab5^{DN}$ or $Vps4^{DN}$ ddaC neurons (Figure S4E; data not shown).

Thus, Rab5 and ESCRT-mediated endocytic pathways regulate proper distribution of the cell-surface molecules Nrg, Robo, and N-Cad in ddaC neurons.

Nrg Is Localized on Endosomes in Wild-Type ddaC Neurons and Downregulated prior to Dendrite Pruning

We next investigated the dynamics of Nrg, Robo, and N-Cad proteins in wild-type ddaC neurons at various stages of dendrite growth and pruning. Interestingly, Nrg, rather than Robo and N-Cad, was dramatically redistributed from plasma membrane to endosomal compartments before the onset of dendrite pruning (Figures 5A, 5B, and 5C; data not shown). In wild-type ddaC neurons, Nrg was localized around the cortex of the somas, dendrites, and axons at wL3 and WP stages (n = 17 and 10, respectively; Figures 5A and 5B). The onset of dendrite pruning occurred approximately at 6 hr APF with many swellings forming along the dendrites, whereas the majority of the dendrites were still attached to the ddaC somas (Figures 5C and 6I; Kirilly et al., 2009). Importantly, Nrg was redistributed to numerous intracellular punctate structures at 6 hr APF in all ddaC neurons (n = 15; 100%; Figure 5C), occurring concomitantly with its drastically reduced intensity in the somas, dendrites, and axons at 6 hr APF (Figure 5D). GFP-2xFYVE, which predominantly marks early endosomal compartments (Wucherpfennig et al., 2003), was used to determine whether Nrg-positive puncta are distributed on early endosomes. At wL3 and WP stages, Nrg protein was primarily localized on the plasma membrane and exhibited little overlap with GFP-2xFYVE puncta in the cytoplasm (n = 32 and 27; Figures 5E and 5F). However, Nrg-positive puncta were predominantly colocalized with GFP-2xFYVE signals at 6 hr APF in ddaC neurons (n = 30; Figure 5G). We observed the redistribution of Nrg on GFP-2xFYVE-positive endosomes as early as 3 hr APF (data not shown). Moreover, many Nrg puncta were also colocalized with the late endosome/lysosomal marker LAMP1-GFP in ddaC neurons at 6 hr APF (n = 10; Figure S5C), suggesting that Nrg may be transported toward late endosomes for lysosomal degradation. We also observed that early endosomes were often positive for LAMP1-GFP in ddaC neurons at 6 hr APF (n = 10; data not shown), suggesting a progressive transition from early to late endosomes (Rink et al., 2005). Thus, Nrg is distributed on the endosomal compartments in ddaC neurons prior to dendrite pruning.

We next ascertained whether Nrg levels are elevated in *Rab5* and *ESCRT* mutant ddaC neurons at 6 hr APF prior to the onset

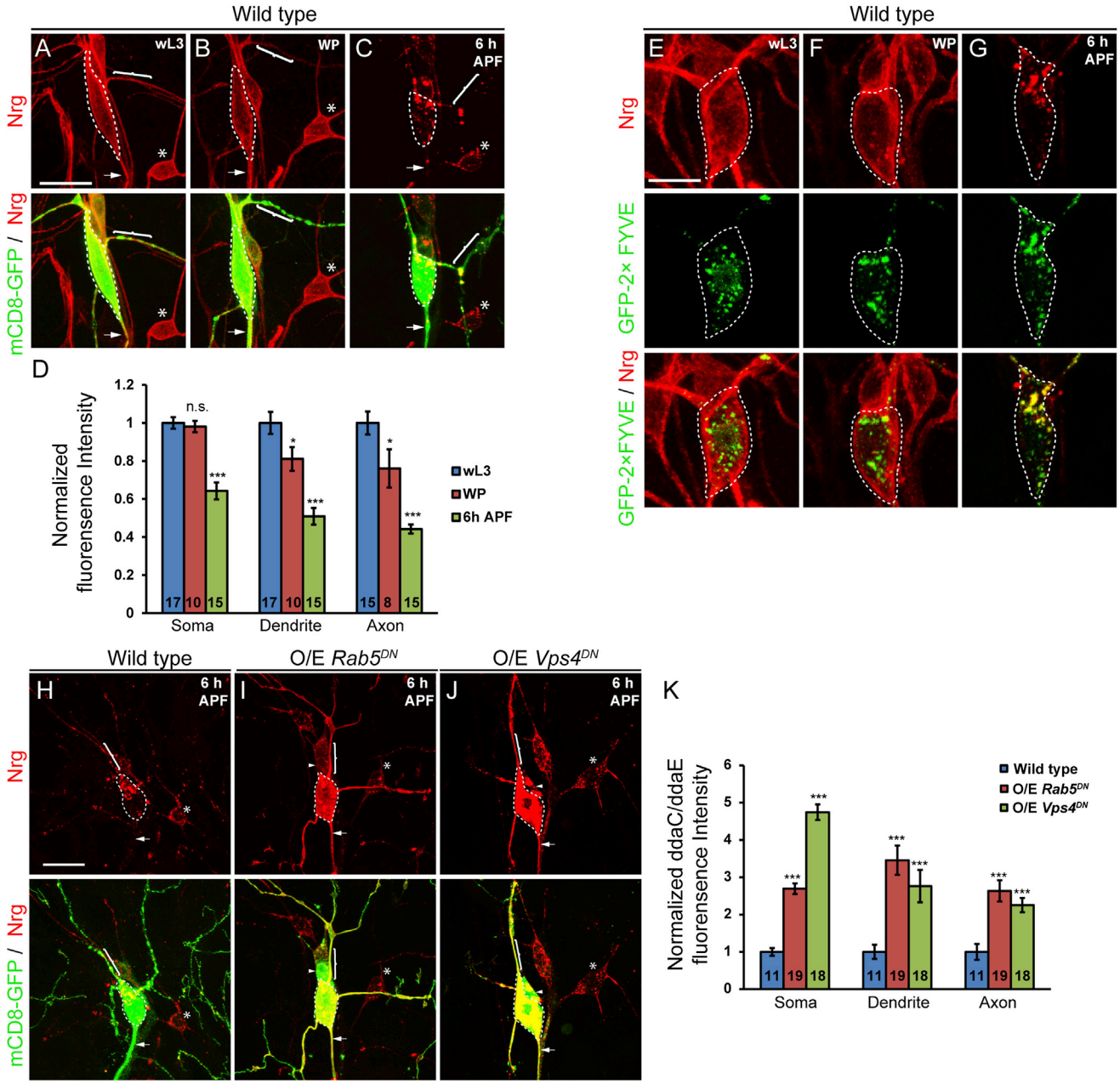

Figure 5. Nrg Is Localized on Endosomes in Wild-Type ddaC Neurons and Downregulated prior to Dendrite Pruning

(A–C) The dynamic distribution of Nrg in ddaC neurons at wL3 (A), WP (B), and 6 hr APF (C).

(D) Quantification of Nrg immunostaining intensity.

(E–G) The distribution of Nrg and GFP-2xFYVE in ddaC neurons at wL3 (E), WP (F), and 6 hr APF (G) stages.

(H–J) The distribution of Nrg in wild-type (H), *Rab5*^{DN} (I), or *Vps4*^{DN} (J) ddaC neurons at 6 hr APF. White arrowheads point to apoptotic ddaF neurons also labeled by the stronger *ppk-Gal4* driver (Chr II). ddaC somas are marked by dashed lines, axons by arrows, and proximal dendrites by curly brackets. ddaE somas are marked by asterisks.

(K) Quantification of Nrg immunostaining intensity.

Error bars represent SEM. The scale bars in (A) and (H) represent 20 μm, and the scale bar in (E) represents 10 μm. See genotypes of fly strains in Supplemental Experimental Procedures. See also Figure S5.

of dendrite pruning. Notably, Nrg protein levels were dramatically increased in the neuronal compartments of *Rab5*^{DN} (n = 19; Figure 5I) or *Vps4*^{DN} (n = 18; Figure 5J) ddaC neurons at 6 hr APF, compared to the wild-type controls (n = 11; Figure 5H). At 6 hr APF, we also observed Nrg enrichment on the cell surface (3.2-fold increase) and the enlarged endosomal compartments in *Rab5*^{DN} ddaC neurons (Figure 5I), similar to that at wL3 stage (Figure 4B). Moreover, Nrg puncta were

completely colocalized with LAMP1-GFP and robustly accumulated on these enlarged late endosomes in all $Rab5^{DN}$ or $Vps4^{DN}$ mutant neurons (n = 12 and 10, respectively; Figure S5C; data not shown), indicative of a severe defect in endosomal distribution or trafficking of Nrg. When $Rab5^{DN}$ or $Vps4^{DN}$ expression was induced at the late larval stage via the Gene-Switch system, we also observed robust accumulations of Nrg on enlarged endosomes at 6 hr APF in $Rab5^{DN}$ (62%; n = 13) or $Vps4^{DN}$ (79%; n = 19) mutant ddaC neurons (Figure S5B). At WP stage, we observed no or little accumulation of Nrg on endosomes in $Rab5^{DN}$ (n = 20) or $Vps4^{DN}$ (n = 5) mutant ddaC neurons (Figure S5B). Given that Nrg is drastically distributed on endosomes in wild-type ddaC neurons at 6 hr APF, these observations further suggest active endosomal trafficking of Nrg before the onset of dendrite pruning. In contrast, downregulation of Nrg appears not to occur in the CNS neurons. Whereas the endosomal compartments were enlarged and ubiquitin-positive (Figure S5D; data not shown), no Nrg aggregates were observed in mutant MB γ neurons (Figure S5D) or ventral nerve cord (VNC) neurons (data not shown) devoid of *Rab5* or *Vps4* function, suggesting no or little endocytosis and turnover of Nrg in the CNS neurons. Thus, these results indicate a specific requirement of Nrg downregulation in ddaC sensory neurons before the onset of dendrite pruning.

Taken together, the L1-type CAM Nrg is downregulated in ddaC neurons via the endolysosomal pathway in ddaC neurons prior to dendrite pruning.

Overexpression of Nrg Alone Is Sufficient to Inhibit Dendrite Pruning in ddaC Neurons

Given that Nrg is downregulated via Rab5/ESCRT-dependent endocytic pathways prior to dendrite pruning, we next investigated whether overexpression of Nrg inhibits ddaC dendrite pruning and phenocopies *Rab5* or *ESCRT* mutants. Importantly, Nrg overexpression alone is sufficient to inhibit dendrite pruning in ddaC neurons, similar to those in *Rab5* or *ESCRT* mutants. When the neuron-specific Nrg isoform (Nrg180) was overexpressed at lower levels via either of two independent *nrg* transgenes, namely *UAS-Nrg* (Islam et al., 2003) and *UAS-Nrg-EGFP* (Enneking et al., 2013), ddaC neurons exhibited consistent dendrite-severing (38% and 38%, respectively) or severe fragmentation (42% and 54%, respectively) defects at 16 hr APF (n = 24 and 24, respectively; Figure S6B). High-level expression of Nrg (n = 23; Figure 6B) or Nrg-EGFP (n = 24; Figure 6C) resulted in stronger dendrite-severing defects (87% and 90%, respectively) with the persistence of 4.0 and 3.9 primary and secondary dendrites attached to ddaC somas (Figures 6G and 6H). Overexpressed Nrg was distributed in the somas, dendrites, and axons of ddaC neurons at 6 hr APF (data not shown). Overexpression of Nrg in either glia or epidermal cells did not enhance the dendrite-severing defects caused by overexpression of Nrg within ddaC neurons (n = 39 and n = 46; data not shown), suggesting that homotypic interaction of Nrg between ddaC neuron and glia/epidermal cells may not be important for the regulation of dendrite pruning. As a control, neither Robo nor N-Cad overexpression resulted in any pruning defects in ddaC neurons (n = 16 and 16, respectively; data not shown), underscoring a specific role of Nrg among these cell-surface molecules in inhibiting dendrite pruning. Thus, these overexpression results further support the notion that downregulation of Nrg is a prerequisite for triggering dendrite pruning in ddaC neurons.

The extracellular domain (ECD) of Nrg contains six immunoglobulin (Ig) and five FnIII domains whereas its intracellular domain (ICD) contains FERM-binding domain, ankrin-binding domain (ABD), and PDZ-binding domain (PBD) (Figure S6A). Overexpression of the truncated Nrg protein lacking the entire ICD ($Nrg^{\Delta ICD}$), like the full-length Nrg, led to dendrite-pruning defects in ddaC neurons (n = 16; Figures 6D, 6G, and 6H). Similarly, overexpression of $Nrg^{\Delta ABD}$ lacking the ABD domain (n = 24; Figure 6E) or $Nrg^{\Delta ABD+PBD}$ lacking both ABD and PBD domains (n = 31; Figure 6F) also inhibited ddaC dendrite pruning (Figures 6G and 6H). These data suggest that the ECD of Nrg is important for its function in inhibiting dendrite pruning, whereas the ABD and PBD domains are dispensable.

Loss of *nrg* Function Results in Precocious Dendrite Pruning with Intact Axonal Architecture in ddaC Neurons

Because initiation of ddaC dendrite pruning requires Nrg downregulation, we assessed whether loss of *nrg* function results in dendrite pruning at an early time point. We generated homozygous MARCM clones using the previously reported null allele nrg^{14} (Hortsch et al., 1990) and compared them with wild-type clones from the *FRT19A* control. At 6 hr APF, wild-type ddaC neurons retained the majority of their larval dendrites (n = 29; Figure 6I). An average of 10.1 primary and secondary dendrites were connected to their ddaC somas (Figure 6O). Importantly, all nrg^{14} MARCM ddaC neurons, which eliminated Nrg protein (n = 5; wild-type, n = 10; Figure S6C), exhibited precocious dendrite-pruning defects (n = 47; Figures 6J and 6O). Only 1.6 of primary and secondary dendrites remained attached to the nrg^{14} ddaC somas (Figure 6J). Severing and removal of ddaC dendrites in nrg^{14} ddaC neurons occurred at 4 hr and 5 hr APF (Figure S6D). Thus, loss of *nrg* function leads to ddaC dendrite pruning occurring at the earlier time point. Formation of major dendrites was slightly affected in nrg^{14} mutant ddaC neurons (n = 35; Figure 6J), whereas elaboration of high-order dendrite branches was apparently reduced (n = 3; data not shown), similar to that in *nrg* RNAi knockdown (Yang et al., 2011). We also observed that all nrg^{14} mutant ddaC neurons exhibited compartmentalized calcium transients between 4 and 4.5 hr APF (n = 9; 100%; Movie S2), whereas only 25% of the wild-type neurons showed calcium transients during the same period (n = 12; Movie S1). Because compartmentalized calcium transients act as temporal and spatial cues to trigger dendrite pruning (Kanamori et al., 2013), the earlier occurrence of calcium transients further supports the precocious pruning phenotype in nrg^{14} mutants.

We next conducted a rescue experiment to confirm the specificity of the precocious pruning phenotype caused by loss of *nrg* function. To this end, we utilized a Pacman-based genomic rescue transgene *P*[*nrg_wt*] to express Nrg protein at the endogenous level (Enneking et al., 2013) in nrg^{14} MARCM ddaC neurons (n = 5; Figure S6C). Importantly, the expression of Nrg fully rescued the precocious pruning phenotype (n = 10; Figures 6K and 6O) and restored the dendritic morphology in nrg^{14} ddaC neurons (n = 11; Figures 6K and 6O). We also conducted the rescue experiment with the genomic rescue transgene *P*

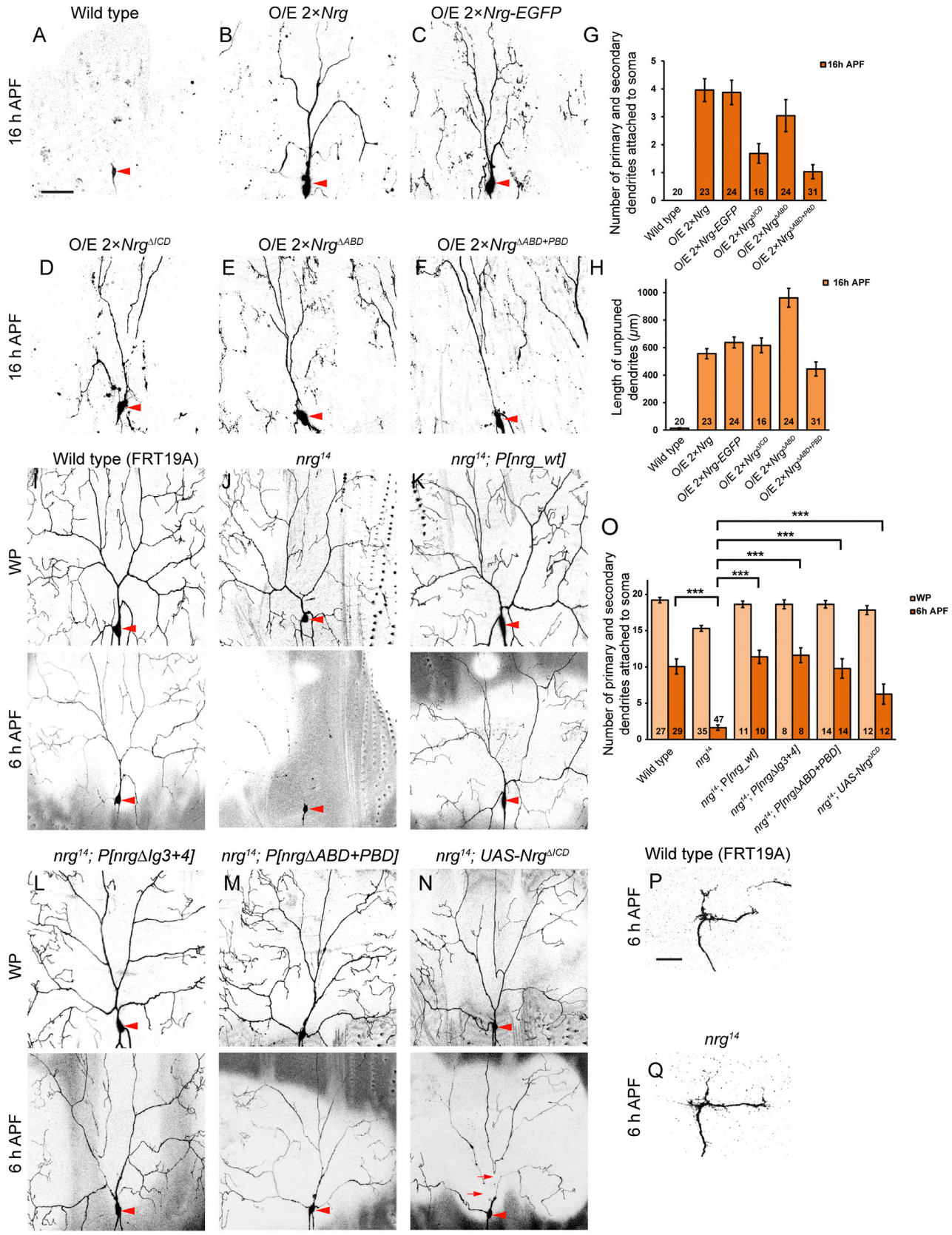

(legend on next page)

[*nrgΔIg3+4*] deleting the extracellular Ig domains 3 and 4, which completely disrupt the Nrg homotypic interaction (Enneking et al., 2013). *P*[*nrgΔIg3+4*] fully rescued nrg^{14}-null mutant in terms of the premature pruning (n = 8; Figures 6L and 6O), suggesting the Nrg homotypic interaction might not be important for inhibiting dendrite pruning. Interestingly, the genomic rescue transgene *P*[*nrgΔABD+PBD*] lacking both ABD and PBD domains (n = 14; Figures 6M and 6O), *P*[*nrgΔABD*] lacking the ABD (n = 13; data not shown), or *P*[*nrgΔPBD*] lacking the PBD (n = 10; data not shown) fully rescued the nrg^{14} mutant phenotype. Moreover, overexpression of $Nrg^{\Delta ICD}$ lacking the entire ICD partially but significantly rescued the nrg^{14} premature pruning phenotype (n = 12; Figures 6N and 6O), suggesting that the ECD of Nrg is important for its function in stabilizing dendrites and/or inhibiting pruning, likely via its adhesive property.

To rule out the possibility that Nrg plays a general role in stabilizing axonal and dendritic architectures in ddaC neurons, we investigated whether loss of *nrg* function affects the connectivity between the ddaC axonal termini and the VNC. Interestingly, all the axonal termini of nrg^{14} ddaC neurons (n = 14; Figure 6Q) exhibited normal morphology and proper connection with the VNC at 6 hr APF, similar to those of wild-type neurons (n = 11; Figure 6P), suggesting that Nrg is dispensable for stabilization of the axonal structure and connectivity in ddaC neurons.

Collectively, these results indicate an important role of Nrg in stabilizing the dendrites, but not the axons, in ddaC sensory neurons.

Rab5 and ESCRT Restrain Nrg Function to Promote ddaC Dendrite Pruning

We further investigated whether robust accumulation of Nrg in *Rab5* or *ESCRT* mutant ddaC neurons is functionally relevant to the dendrite-pruning defects. To this end, we tested whether attenuation of *nrg* function could suppress the dendrite-pruning defects in *Rab5* or *ESCRT* mutant ddaC neurons. Importantly, the expression of two independent *nrg* RNAi transgenes, both shown to efficiently eliminate Nrg proteins (Figure 4D; data not shown), drastically mitigated the dendrite-pruning phenotypes in $Rab5^{DN}$ ddaC neurons (Figures 7B–7E). Compared to 4.5 primary and secondary dendrites in the $Rab5^{DN}$ control (n = 30; Figures 7A and 7D), the expression of either of *nrg* RNAi constructs resulted in an average of 0.6 and 0.6 primary and secondary dendrites connected to the $Rab5^{DN}$ ddaC neurons, respectively (n = 14 and 16, respectively; Figures 7B, 7C, and 7D). Moreover, the severing of major dendrites, an initiation step of dendrite pruning, also occurred in the suppression experiments (Figure S7A). Consistently, Nrg knockdowns, via these *nrg* RNAi transgenes, also significantly suppressed the dendrite-pruning phenotypes in $Vps4^{DN}$ ddaC neurons (n = 23 and 31, respectively; Figures 7G–7J), compared to the $Vps4^{DN}$ control (n = 39; Figures 7F, 7I, and 7J). Notably, Nrg RNAi knockdowns in $Rab5^{DN}$ ddaC neurons displayed 28% (no. 1) and 38% (no. 2) penetrance of the severing defects, compared with 93% penetrance in the $Rab5^{DN}$ control. Similarly, $Vps4^{DN}$ ddaC neurons with either of Nrg knockdowns (33% and 42%, respectively) showed lower penetrance of the severing defects than the $Vps4^{DN}$ control (72%). In contrast, RNAi knockdown of either Robo or N-Cad, which also eliminated their respective proteins (Figures S4C and S4D), failed to suppress the $Rab5^{DN}$ or $Vps4^{DN}$ dendrite-pruning phenotypes at 16 hr APF (n = 20 and 16, respectively; Figure S7D; data not shown). As a control, Nrg, Robo, or N-Cad knockdowns did not lead to dendrite-pruning defects in ddaC neuron at 16 hr APF (data not shown). Moreover, when $Rab5^{DN}$ or $Vps4^{DN}$ was overexpressed in nrg^{14} mutant ddaC neurons, we did not observe any precocious dendrite-pruning defects at 6 hr APF (n = 12 and 11, respectively; Figure S7B; data not shown), compared to the nrg^{14} mutant neurons (Figure 6J). Thus, these data suggest that Nrg is unlikely the only target for Rab5 and ESCRT. Knockdown of Nrg significantly suppressed the dendrite-pruning defects in EcR^{DN} (n = 47), Brm^{DN} (n = 28), or *CBP* RNAi ddaC neurons (n = 24; Figure S7C), suggesting that *nrg* acts downstream of these genes during pruning.

Moreover, overexpression of either Nrg or Nrg-EGFP caused significant enhancement of the $Rab5^{DN}$ or $Vps4^{DN}$ dendrite-pruning defects at 16 hr APF. Compared to 4.2 primary and secondary dendrites in the $Rab5^{DN}$ control (n = 47; Figures 7K and 7Q), Nrg (n = 41; Figures 7L and 7Q) or Nrg-EGFP (n = 38; Figures 7M and 7Q) expression resulted in an average of 5.8 or 6.0 primary/secondary dendrites attached to the $Rab5^{DN}$ ddaC neurons, respectively. Moreover, Nrg or Nrg-EGFP expression significantly enhanced the $Vps4^{DN}$-pruning phenotypes. Compared to 1.3 primary and secondary dendrites in the $Vps4^{DN}$ control (n = 16; Figures 7N and 7Q), Nrg (n = 22; Figures 7O and 7Q) or Nrg-EGFP (n = 20; Figures 7P and 7Q) expression caused strong enhancement of the $Vps4^{DN}$ dendrite-pruning phenotype with an average of 3.3 or 5.9 primary/secondary dendrites attached. Consistently, Nrg or Nrg-EGFP expression also significantly enhanced the $Rab5^{DN}$- or $Vps4^{DN}$-pruning phenotypes in terms of the total length of unpruned dendrites (Figure 7R).

Thus, these epistasis results demonstrate that Rab5 and ESCRT restrain the inhibitory function of Nrg to facilitate dendrite pruning in ddaC neurons.

Figure 6. Overexpression of Nrg Alone Is Sufficient to Inhibit Dendrite Pruning, whereas Loss of *nrg* Function Results in Precocious Dendrite Pruning with Intact Axonal Architecture in ddaC Neurons

(A–F) Dendrites of wild-type (A), O/E Nrg (B), O/E Nrg-EGFP (C), O/E $Nrg^{\Delta ICD}$ (D), O/E $Nrg^{\Delta ABD}$ (E), or O/E $Nrg^{\Delta ABD+PBD}$ (F) ddaC neurons at 16 hr APF.

(G) Quantification of the average number of primary and secondary ddaC dendrites.

(H) Quantification of the total length of unpruned ddaC dendrites.

(I–N) Dendrites of ddaC neurons from wild-type (FRT 19A) (I), nrg^{14} MARCM (J), nrg^{14} with Nrg expression (K), nrg^{14} with $Nrg^{\Delta Ig3+4}$ expression (L), nrg^{14} with $Nrg^{\Delta ABD+PBD}$ expression (M), and nrg^{14} with $Nrg^{\Delta ICD}$ expression (N) at WP and 6 hr APF. Red arrows point to proximal severing of the dorsal dendrite branches.

(O) Quantification of the average number of primary and secondary ddaC dendrites.

(P and Q) Axonal termini of wild-type (P) and nrg^{14} (Q) at 6 hr APF.

Error bars represent SEM. The scale bar in (A) represents 50 μm and in (P) represents 25 μm. See genotypes of fly strains in Supplemental Experimental Procedures. See also Figure S6.

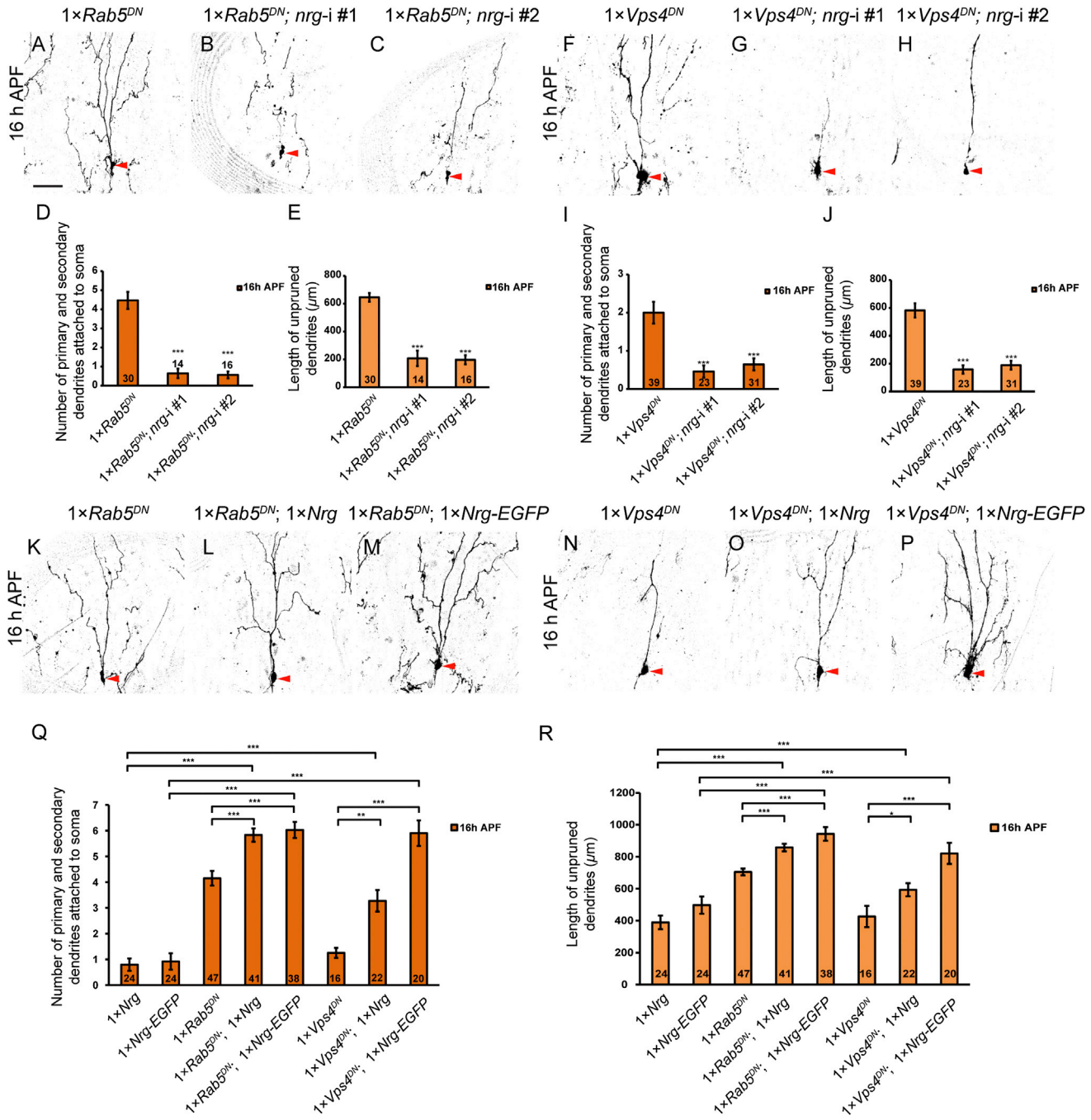

Figure 7. Rab5 and ESCRT Restrain Nrg Function to Promote ddaC Dendrite Pruning

(A–C) Dendrites of *Rab5*^{DN} ddaC neurons coexpressing the Mical$^{N\text{-}ter}$ control (A) or Nrg RNAi no. 1 (B) or no. 2 (C) at 16 hr APF.

(D) Quantification of the average number of primary and secondary ddaC dendrites.

(E) Quantification of the total length of unpruned ddaC dendrites.

(F–H) Dendrites of *Vps4*^{DN} ddaC neurons coexpressing the Mical$^{N\text{-}ter}$ control (F) or Nrg RNAi no. 1 (G) or no. 2 (H) at 16 hr APF.

(I) Quantification of the average number of primary and secondary ddaC dendrites.

(J) Quantification of the total length of unpruned ddaC dendrites.

(K–M) Dendrites of *Rab5*^{DN} ddaC neurons coexpressing the Mical$^{N\text{-}ter}$ control (K), Nrg (L), or Nrg-EGFP (M) at 16 hr APF.

(N–P) Dendrites of *Vps4*^{DN} ddaC neurons coexpressing the Mical$^{N\text{-}ter}$ control (N), Nrg (O), or Nrg-EGFP (P) at 16 hr APF.

(Q) Quantification of the average number of primary and secondary ddaC dendrites.

(R) Quantification of the total length of unpruned ddaC dendrites.

Error bars represent SEM. The scale bar represents 50 μm. See genotypes of fly strains in Supplemental Experimental Procedures. See also Figure S7.

DISCUSSION

A Cell-Autonomous Role of the Endocytic Pathways in Dendrite Pruning

Endocytic pathways profoundly regulate turnover and homeostasis of various cell-surface adhesion proteins and guidance receptors in the developing nervous systems (O'Donnell et al., 2009; Sann et al., 2009). Perturbation of endocytic pathways often leads to a variety of neurodegenerative diseases, such as frontotemporal dementia, amyotrophic lateral sclerosis, Alzheimer's disease, lysosomal storage diseases, and Niemann-Pick disease (Nixon et al., 2008). In *Drosophila*, the endolysosomal pathway is activated in neighboring glia to engulf degenerating axon/dendrite fragments for their subsequent breakdown during pruning, suggesting a non-cell-autonomous role (Awasaki and Ito, 2004; Han et al., 2011; Watts et al., 2004). Here, we report that Rab5 and the ESCRT complexes, two key endocytic regulators, cell autonomously promote dendrite pruning in ddaC neurons. Consistent with our findings, the endocytic pathways also play a cell-autonomous role in axon pruning of MB γ neurons (O. Schuldiner, personal communication). How do Rab5/ESCRT-dependent endocytic pathways facilitate dendrite pruning in ddaC neurons at the cellular level? Here, we have identified a cell-surface adhesion protein, namely the L1-type CAM Nrg, as a target of Rab5/ESCRT-dependent endocytic pathways.

An Inhibitory Role of Nrg in Dendrite Pruning

Drosophila Nrg and the mammalian L1-type CAMs regulate axonal growth and guidance (Hortsch et al., 1990; Maness and Schachner, 2007), synaptic stability and function (Enneking et al., 2013; Godenschwege et al., 2006), and axon/dendrite morphogenesis (Goossens et al., 2011; Yamamoto et al., 2006; Yang et al., 2011). Mutations in the human L1 CAM gene have been reported to cause a broad spectrum of neuronal disorders (Kenwrick et al., 2000; Maness and Schachner, 2007). In this study, we identified the *Drosophila* L1-type CAM Nrg as the key cell-surface molecule that inhibits dendrite pruning in ddaC neurons. The extracellular domains of the L1-type CAMs can regulate cell-cell adhesion via homophilic and/or heterophilic interactions, whereas their intracellular domains can link the proteins with F-actin/spectrins to stabilize the cytoskeletal architecture (Hortsch, 2000). In *C. elegans*, a ligand-receptor complex of cell adhesion molecules containing the nematode Nrg homolog controls dendrite-substrate adhesion to stabilize and pattern dendritic arbors in certain sensory neurons (Dong et al., 2013; Salzberg et al., 2013). In *Drosophila*, Nrg-mediated cell adhesion plays an essential role in stabilizing synapse growth and maintenance at the larval neuromuscular junction (Enneking et al., 2013). Likewise, Nrg may also mediate adhesion of the dendrites to their adjacent epidermis to stabilize the dendritic architecture in ddaC sensory neurons, whereas downregulation of Nrg may reduce dendritic adhesion/stability and result in disassembly of dendrites. Consistent with the potential adhesive role, our structure-function analysis indicates that the ECD of Nrg is important for its function in stabilizing dendrite and/or inhibiting dendrite pruning in ddaC neurons. The fact that overexpression of the ICD-deleted Nrg protein partially rescued the nrg^{14} mutant phenotype suggests that, in addition to the adhesion function of the ECD, the ICD of Nrg may recruit cytoskeletal components to stabilize dendritic branches in ddaC neurons. We therefore favor the model that the adhesive role of Nrg is a potential mechanism for inhibiting pruning in ddaC sensory neurons.

Another major class of CAMs, integrins, were shown to regulate dendrite-substrate interactions and anchor ddaC dendritic arbors to the extracellular matrix (Han et al., 2012; Kim et al., 2012). However, unlike Nrg, integrins do not accumulate on enlarged endosomes in *Rab5* or *ESCRT* ddaC neurons, implying that integrins are not regulated by Rab5/ESCRT-dependent endocytic pathways in ddaC neurons (this study). Moreover, other cell-surface molecules Robo and N-Cad, albeit regulated by the endolysosomal pathway in motor neurons (Keleman et al., 2002), photoreceptors (Williamson et al., 2010), or sensory neurons (this study), are dispensable for normal progression of dendrite pruning in ddaC neurons. Thus, this study highlights an important role of the L1-type CAM Nrg in inhibiting dendrite pruning of ddaC sensory neurons.

Interestingly, loss of *nrg* function causes precocious dendrite pruning without affecting the axonal integrity and connectivity in ddaC neurons, underscoring a specific requirement of Nrg in stabilizing the dendrites, but not the axons. Downregulation of Nrg may reduce dendritic adhesive properties of ddaC sensory neurons and thereby make the dendritic architecture more susceptible to pruning. It is conceivable that Nrg-independent mechanisms may be utilized to protect the axonal structure from the pruning machinery in ddaC neurons. Moreover, both *nrg* loss of function and gain of function did not affect axon pruning in MB γ neurons (data not shown), further supporting the conclusion that Nrg plays a specific role in dendrite pruning in ddaC sensory neurons. Future studies may elucidate whether and how Nrg mediates its dendritic adhesive properties to inhibit dendrite pruning.

In summary, we show that Rab5/ESCRT-dependent endocytic pathways facilitate dendrite pruning of ddaC neurons by downregulating the *Drosophila* L1-type CAM Nrg during early metamorphosis. We demonstrate the role of the cell-surface adhesion protein Nrg in inhibiting dendrite pruning in ddaC sensory neurons. Thus, this study opens the door for further studies of the functions of cell-surface molecules in the regulation of dendritic adhesion during neuronal remodeling.

EXPERIMENTAL PROCEDURES

Fly Strains

The following fly stocks were used in this study: $Rab5^{2}$ (M. Gonzalez-Gaitan), $Vps28^{B9}$ (D. Bilder), $Vps32^{G5}$ (D. Bilder), avl^{1} (D. Bilder), *UAS-GFP-Rab5* (M. Gonzalez-Gaitan), $UAS\text{-}Rab5^{DN}$ (M. Gonzalez-Gaitan), and $UAS\text{-}Vps4^{DN}$ (H. Stenmark). The details about the fly strains can be found in the Supplemental Information.

Generation of UAS-$Nrg^{\Delta ICD}$ and $Nrg^{\Delta ABD+PBD}$ Transgenes

The GATEWAY pTWF vector containing a fragment of the *nrg* cDNA (encoding amino acids [aas] 1–1,157 and aas 1-1,223) were constructed, and several transgenic lines were established by the Bestgene.

MARCM Analysis of ddaC Neurons

We carried out MARCM analysis, dendrite imaging, and quantification as previously described (Kirilly et al., 2009). See the Supplemental Information for the details.

Statistical Analysis

Statistical significance was determined using two-tailed Student's test. Error bars in all experiments represent SEM. Significance was defined as ***p < 0.001, **p < 0.01, *p < 0.05, and not significant (n.s.) in all graphs.

Time-Lapse Calcium Imaging

Calcium imaging was performed with microLAMBDA spinning disk using a microscope (Plan Apo oil objective; 40× numerical aperture = 1.4; Nikon) equipped with a spinning-disk confocal unit Yokogawa CSU-X1 (Yokogawa) and a sCMOS digital camera (ORCA-Flash4.0, Hamamatsu Photonics). GCaMP3 fluorescence was collected from eight to ten optical sections at 1.5 μm thickness (exposure time 150–180 ms) without interval. Obtained images were analyzed using Metamorph (Molecular Devices) and Fiji software (Schindelin et al., 2012).

Dissection of Brains, Visualization of CNS Neurons, and MARCM Mosaic Analysis

Late wL3 larval brains were dissected in PBS and fixed in 4% formaldehyde for 20 min. Brains were washed in PBS + 1% Triton X for three times for 10 min each. For the clonal analysis study (MARCM), embryos were collected at 6 hr interval. The clones were induced in the first instar larvae with 1 hr heat shock at 39°C. *201Y-Gal4* labels postmitotic γ neurons.

Quantification of Immunolabeling

To quantify the immunolabeling intensities of Nrg at wL3/WP/6 hr (Figure 5D), soma/dendrite/axon regions were drawn on the appropriate fluorescent channel according to the GFP channel in ImageJ. After the background subtraction (rolling ball radius = 50), we measured the mean gray value of Nrg in the marked areas and normalized to that at wL3 stage. To quantify the ddaC/ddaE relative immunolabeling intensities ratio of Nrg (Figure 5K), soma/dendrite/axon regions were drawn on the appropriate fluorescent channel according to the GFP channel in ImageJ. After subtracting the background (rolling ball radius = 50) on the entire image of that channel, we measured the mean gray value in the marked areas in ddaC or ddaE on the same images and calculated their ratios. The ratios were normalized to corresponding average control values and subjected to statistical t test for comparison. Graphs display the average values of ddaC/ddaE ratios. The number of samples (n) in each group is shown on the bars.

Quantification of ddaC Dendrites

Live confocal images of ddaC neurons expressing *UAS-mCD8-GFP* driven by *ppk-GAL4* were shown at WP, 6 hr APF, and 16 hr APF. The average number of primary and secondary dendrites attached to soma was counted from wild-type or mutant ddaC neurons. The total length of unpruned dendrites was measured using Image J. The number of samples (n) in each group is shown on the bars. Dorsal is up in all images.

SUPPLEMENTAL INFORMATION

Supplemental Information includes Supplemental Experimental Procedures, seven figures, two tables, and two movies and can be found with this article online at http://dx.doi.org/10.1016/j.devcel.2014.06.014.

AUTHOR CONTRIBUTIONS

F.Y., H.W., H.Z., and Y.W. conceived and designed the study. H.Z. and Y.W. equally performed the work. J.J.L.W. helped to measure the Nrg levels. H.Z., Y.W., K.-L.L., Y.-C.L., H.W., and F.Y. analyzed the data. F.Y., Y.W., and H.Z. wrote the paper.

ACKNOWLEDGMENTS

We thank O. Schuldiner and K. Emoto for communicating results prior to publications. We thank S. Artavanis-Tsakonas, K. Basler, H. Bellen, D. Bilder, S. Bray, S. Cohen, B. Dickson, M. Gonzalez-Gaitan, J. Hooper, Y.N. Jan, H. Keshishian, T. Klein, A.L. Kolodkin, T. Kornberg, H. Kramer, B. Limbourg-Bouchon, M. O'Connor, J. Pielage, P. Rorth, O. Schuldiner, H. Steller, H. Stenmark, J. Tamkun, T. Uemura, the Bloomington Stock Center (BSC), DSHB (University of Iowa), and VDRC (Austria) for generously providing antibodies and fly stocks. We thank members of the F.Y. laboratory for helpful assistance. We also thank M. Calvert from the TLL microscopy facility and N. Bogard for technical assistance. Y.W. and J.J.L.W. are recipients of the NGS postgraduate scholarship, Singapore. This work was supported by Temasek Life Sciences Laboratory (TLL), Singapore (to F.Y.).

Received: December 9, 2013
Revised: April 23, 2014
Accepted: June 17, 2014
Published: August 25, 2014

REFERENCES

Awasaki, T., and Ito, K. (2004). Engulfing action of glial cells is required for programmed axon pruning during Drosophila metamorphosis. Curr. Biol. *14*, 668–677.

Bagri, A., Cheng, H.J., Yaron, A., Pleasure, S.J., and Tessier-Lavigne, M. (2003). Stereotyped pruning of long hippocampal axon branches triggered by retraction inducers of the semaphorin family. Cell *113*, 285–299.

Castellani, V., Falk, J., and Rougon, G. (2004). Semaphorin3A-induced receptor endocytosis during axon guidance responses is mediated by L1 CAM. Mol. Cell. Neurosci. *26*, 89–100.

Ceresa, B.P., and Schmid, S.L. (2000). Regulation of signal transduction by endocytosis. Curr. Opin. Cell Biol. *12*, 204–210.

Dietzl, G., Chen, D., Schnorrer, F., Su, K.C., Barinova, Y., Fellner, M., Gasser, B., Kinsey, K., Oppel, S., Scheiblauer, S., et al. (2007). A genome-wide transgenic RNAi library for conditional gene inactivation in Drosophila. Nature *448*, 151–156.

Dittman, J., and Ryan, T.A. (2009). Molecular circuitry of endocytosis at nerve terminals. Annu. Rev. Cell Dev. Biol. *25*, 133–160.

Dong, X., Liu, O.W., Howell, A.S., and Shen, K. (2013). An extracellular adhesion molecule complex patterns dendritic branching and morphogenesis. Cell *155*, 296–307.

Enneking, E.M., Kudumala, S.R., Moreno, E., Stephan, R., Boerner, J., Godenschwege, T.A., and Pielage, J. (2013). Transsynaptic coordination of synaptic growth, function, and stability by the L1-type CAM Neuroglian. PLoS Biol. *11*, e1001537.

Entchev, E.V., Schwabedissen, A., and González-Gaitán, M. (2000). Gradient formation of the TGF-beta homolog Dpp. Cell *103*, 981–991.

Fournier, A.E., Nakamura, F., Kawamoto, S., Goshima, Y., Kalb, R.G., and Strittmatter, S.M. (2000). Semaphorin3A enhances endocytosis at sites of receptor-F-actin colocalization during growth cone collapse. J. Cell Biol. *149*, 411–422.

Godenschwege, T.A., Kristiansen, L.V., Uthaman, S.B., Hortsch, M., and Murphey, R.K. (2006). A conserved role for Drosophila Neuroglian and human L1-CAM in central-synapse formation. Curr. Biol. *16*, 12–23.

Goossens, T., Kang, Y.Y., Wuytens, G., Zimmermann, P., Callaerts-Végh, Z., Pollarolo, G., Islam, R., Hortsch, M., and Callaerts, P. (2011). The Drosophila L1CAM homolog Neuroglian signals through distinct pathways to control different aspects of mushroom body axon development. Development *138*, 1595–1605.

Grueber, W.B., Ye, B., Moore, A.W., Jan, L.Y., and Jan, Y.N. (2003). Dendrites of distinct classes of Drosophila sensory neurons show different capacities for homotypic repulsion. Curr. Biol. *13*, 618–626.

Han, C., Jan, L.Y., and Jan, Y.N. (2011). Enhancer-driven membrane markers for analysis of nonautonomous mechanisms reveal neuron-glia interactions in Drosophila. Proc. Natl. Acad. Sci. USA *108*, 9673–9678.

Han, C., Wang, D., Soba, P., Zhu, S., Lin, X., Jan, L.Y., and Jan, Y.N. (2012). Integrins regulate repulsion-mediated dendritic patterning of Drosophila sensory neurons by restricting dendrites in a 2D space. Neuron *73*, 64–78.

Herz, H.M., Chen, Z., Scherr, H., Lackey, M., Bolduc, C., and Bergmann, A. (2006). vps25 mosaics display non-autonomous cell survival and overgrowth, and autonomous apoptosis. Development *133*, 1871–1880.

Hortsch, M. (2000). Structural and functional evolution of the L1 family: are four adhesion molecules better than one? Mol. Cell. Neurosci. *15*, 1–10.

Hortsch, M., Bieber, A.J., Patel, N.H., and Goodman, C.S. (1990). Differential splicing generates a nervous system-specific form of Drosophila neuroglian. Neuron *4*, 697–709.

Islam, R., Wei, S.Y., Chiu, W.H., Hortsch, M., and Hsu, J.C. (2003). Neuroglian activates Echinoid to antagonize the Drosophila EGF receptor signaling pathway. Development *130*, 2051–2059.

Jahn, R., Lang, T., and Südhof, T.C. (2003). Membrane fusion. Cell *112*, 519–533.

Kage, E., Hayashi, Y., Takeuchi, H., Hirotsu, T., Kunitomo, H., Inoue, T., Arai, H., Iino, Y., and Kubo, T. (2005). MBR-1, a novel helix-turn-helix transcription factor, is required for pruning excessive neurites in Caenorhabditis elegans. Curr. Biol. *15*, 1554–1559.

Kanamori, T., Kanai, M.I., Dairyo, Y., Yasunaga, K., Morikawa, R.K., and Emoto, K. (2013). Compartmentalized calcium transients trigger dendrite pruning in Drosophila sensory neurons. Science *340*, 1475–1478.

Keleman, K., Rajagopalan, S., Cleppien, D., Teis, D., Paiha, K., Huber, L.A., Technau, G.M., and Dickson, B.J. (2002). Comm sorts robo to control axon guidance at the Drosophila midline. Cell *110*, 415–427.

Kennedy, M.J., and Ehlers, M.D. (2006). Organelles and trafficking machinery for postsynaptic plasticity. Annu. Rev. Neurosci. *29*, 325–362.

Kenwrick, S., Watkins, A., and De Angelis, E. (2000). Neural cell recognition molecule L1: relating biological complexity to human disease mutations. Hum. Mol. Genet. *9*, 879–886.

Kim, M.E., Shrestha, B.R., Blazeski, R., Mason, C.A., and Grueber, W.B. (2012). Integrins establish dendrite-substrate relationships that promote dendritic self-avoidance and patterning in Drosophila sensory neurons. Neuron *73*, 79–91.

Kirilly, D., Gu, Y., Huang, Y., Wu, Z., Bashirullah, A., Low, B.C., Kolodkin, A.L., Wang, H., and Yu, F. (2009). A genetic pathway composed of Sox14 and Mical governs severing of dendrites during pruning. Nat. Neurosci. *12*, 1497–1505.

Kirilly, D., Wong, J.J., Lim, E.K., Wang, Y., Zhang, H., Wang, C., Liao, Q., Wang, H., Liou, Y.C., Wang, H., and Yu, F. (2011). Intrinsic epigenetic factors cooperate with the steroid hormone ecdysone to govern dendrite pruning in Drosophila. Neuron *72*, 86–100.

Kuo, C.T., Jan, L.Y., and Jan, Y.N. (2005). Dendrite-specific remodeling of Drosophila sensory neurons requires matrix metalloproteases, ubiquitin-proteasome, and ecdysone signaling. Proc. Natl. Acad. Sci. USA *102*, 15230–15235.

Kuo, C.T., Zhu, S., Younger, S., Jan, L.Y., and Jan, Y.N. (2006). Identification of E2/E3 ubiquitinating enzymes and caspase activity regulating Drosophila sensory neuron dendrite pruning. Neuron *51*, 283–290.

Lee, T., and Luo, L. (1999). Mosaic analysis with a repressible cell marker for studies of gene function in neuronal morphogenesis. Neuron *22*, 451–461.

Lee, T., Marticke, S., Sung, C., Robinow, S., and Luo, L. (2000). Cell-autonomous requirement of the USP/EcR-B ecdysone receptor for mushroom body neuronal remodeling in Drosophila. Neuron *28*, 807–818.

Lee, H.H., Jan, L.Y., and Jan, Y.N. (2009). Drosophila IKK-related kinase Ik2 and Katanin p60-like 1 regulate dendrite pruning of sensory neuron during metamorphosis. Proc. Natl. Acad. Sci. USA *106*, 6363–6368.

Lloyd, T.E., Atkinson, R., Wu, M.N., Zhou, Y., Pennetta, G., and Bellen, H.J. (2002). Hrs regulates endosome membrane invagination and tyrosine kinase receptor signaling in Drosophila. Cell *108*, 261–269.

Loncle, N., and Williams, D.W. (2012). An interaction screen identifies headcase as a regulator of large-scale pruning. J. Neurosci. *32*, 17086–17096.

Lu, H., and Bilder, D. (2005). Endocytic control of epithelial polarity and proliferation in Drosophila. Nat. Cell Biol. *7*, 1232–1239.

Luo, L., and O'Leary, D.D. (2005). Axon retraction and degeneration in development and disease. Annu. Rev. Neurosci. *28*, 127–156.

Maness, P.F., and Schachner, M. (2007). Neural recognition molecules of the immunoglobulin superfamily: signaling transducers of axon guidance and neuronal migration. Nat. Neurosci. *10*, 19–26.

Nixon, R.A., Yang, D.S., and Lee, J.H. (2008). Neurodegenerative lysosomal disorders: a continuum from development to late age. Autophagy *4*, 590–599.

O'Donnell, M., Chance, R.K., and Bashaw, G.J. (2009). Axon growth and guidance: receptor regulation and signal transduction. Annu. Rev. Neurosci. *32*, 383–412.

O'Leary, D.D., and Koester, S.E. (1993). Development of projection neuron types, axon pathways, and patterned connections of the mammalian cortex. Neuron *10*, 991–1006.

Raiborg, C., and Stenmark, H. (2009). The ESCRT machinery in endosomal sorting of ubiquitylated membrane proteins. Nature *458*, 445–452.

Riccomagno, M.M., Hurtado, A., Wang, H., Macopson, J.G., Griner, E.M., Betz, A., Brose, N., Kazanietz, M.G., and Kolodkin, A.L. (2012). The RacGAP β2-Chimaerin selectively mediates axonal pruning in the hippocampus. Cell *149*, 1594–1606.

Rink, J., Ghigo, E., Kalaidzidis, Y., and Zerial, M. (2005). Rab conversion as a mechanism of progression from early to late endosomes. Cell *122*, 735–749.

Rusten, T.E., Vaccari, T., Lindmo, K., Rodahl, L.M., Nezis, I.P., Sem-Jacobsen, C., Wendler, F., Vincent, J.P., Brech, A., Bilder, D., and Stenmark, H. (2007). ESCRTs and Fab1 regulate distinct steps of autophagy. Curr. Biol. *17*, 1817–1825.

Rusten, T.E., Vaccari, T., and Stenmark, H. (2012). Shaping development with ESCRTs. Nat. Cell Biol. *14*, 38–45.

Salzberg, Y., Díaz-Balzac, C.A., Ramirez-Suarez, N.J., Attreed, M., Tecle, E., Desbois, M., Kaprielian, Z., and Bülow, H.E. (2013). Skin-derived cues control arborization of sensory dendrites in Caenorhabditis elegans. Cell *155*, 308–320.

Sann, S., Wang, Z., Brown, H., and Jin, Y. (2009). Roles of endosomal trafficking in neurite outgrowth and guidance. Trends Cell Biol. *19*, 317–324.

Satoh, D., Sato, D., Tsuyama, T., Saito, M., Ohkura, H., Rolls, M.M., Ishikawa, F., and Uemura, T. (2008). Spatial control of branching within dendritic arbors by dynein-dependent transport of Rab5-endosomes. Nat. Cell Biol. *10*, 1164–1171.

Schindelin, J., Arganda-Carreras, I., Frise, E., Kaynig, V., Longair, M., Pietzsch, T., Preibisch, S., Rueden, C., Saalfeld, S., Schmid, B., et al. (2012). Fiji: an open-source platform for biological-image analysis. Nat. Methods *9*, 676–682.

Schubiger, M., Wade, A.A., Carney, G.E., Truman, J.W., and Bender, M. (1998). Drosophila EcR-B ecdysone receptor isoforms are required for larval molting and for neuron remodeling during metamorphosis. Development *125*, 2053–2062.

Sweeney, N.T., Brenman, J.E., Jan, Y.N., and Gao, F.B. (2006). The coiled-coil protein shrub controls neuronal morphogenesis in Drosophila. Curr. Biol. *16*, 1006–1011.

Thompson, B.J., Mathieu, J., Sung, H.H., Loeser, E., Rørth, P., and Cohen, S.M. (2005). Tumor suppressor properties of the ESCRT-II complex component Vps25 in Drosophila. Dev. Cell *9*, 711–720.

Truman, J.W. (1990). Metamorphosis of the central nervous system of Drosophila. J. Neurobiol. *21*, 1072–1084.

Vaccari, T., and Bilder, D. (2005). The Drosophila tumor suppressor vps25 prevents nonautonomous overproliferation by regulating notch trafficking. Dev. Cell *9*, 687–698.

Vaccari, T., Rusten, T.E., Menut, L., Nezis, I.P., Brech, A., Stenmark, H., and Bilder, D. (2009). Comparative analysis of ESCRT-I, ESCRT-II and ESCRT-III function in Drosophila by efficient isolation of ESCRT mutants. J. Cell Sci. *122*, 2413–2423.

Watts, R.J., Hoopfer, E.D., and Luo, L. (2003). Axon pruning during Drosophila metamorphosis: evidence for local degeneration and requirement of the ubiquitin-proteasome system. Neuron *38*, 871–885.

Watts, R.J., Schuldiner, O., Perrino, J., Larsen, C., and Luo, L. (2004). Glia engulf degenerating axons during developmental axon pruning. Curr. Biol. *14*, 678–684.

Williams, D.W., and Truman, J.W. (2005). Cellular mechanisms of dendrite pruning in Drosophila: insights from in vivo time-lapse of remodeling dendritic arborizing sensory neurons. Development *132*, 3631–3642.

Williams, D.W., Kondo, S., Krzyzanowska, A., Hiromi, Y., and Truman, J.W. (2006). Local caspase activity directs engulfment of dendrites during pruning. Nat. Neurosci. *9*, 1234–1236.

Williamson, W.R., Yang, T., Terman, J.R., and Hiesinger, P.R. (2010). Guidance receptor degradation is required for neuronal connectivity in the Drosophila nervous system. PLoS Biol. *8*, e1000553.

Wong, J.J., Li, S., Lim, E.K., Wang, Y., Wang, C., Zhang, H., Kirilly, D., Wu, C., Liou, Y.C., Wang, H., and Yu, F. (2013). A Cullin1-based SCF E3 ubiquitin ligase targets the InR/PI3K/TOR pathway to regulate neuronal pruning. PLoS Biol. *11*, e1001657.

Wucherpfennig, T., Wilsch-Bräuninger, M., and González-Gaitán, M. (2003). Role of Drosophila Rab5 during endosomal trafficking at the synapse and evoked neurotransmitter release. J. Cell Biol. *161*, 609–624.

Yamamoto, M., Ueda, R., Takahashi, K., Saigo, K., and Uemura, T. (2006). Control of axonal sprouting and dendrite branching by the Nrg-Ank complex at the neuron-glia interface. Curr. Biol. *16*, 1678–1683.

Yang, W.K., Peng, Y.H., Li, H., Lin, H.C., Lin, Y.C., Lai, T.T., Suo, H., Wang, C.H., Lin, W.H., Ou, C.Y., et al. (2011). Nak regulates localization of clathrin sites in higher-order dendrites to promote local dendrite growth. Neuron *72*, 285–299.

Yap, C.C., and Winckler, B. (2012). Harnessing the power of the endosome to regulate neural development. Neuron *74*, 440–451.

Zerial, M., and McBride, H. (2001). Rab proteins as membrane organizers. Nat. Rev. Mol. Cell Biol. *2*, 107–117.